Eur. Phys. J. D (2015) 69: 192
DOI: 10.1140/epjd/e2015-60102-0

THE EUROPEAN PHYSICAL JOURNAL D

Regular Article

Double differential electron emission from N_2 under impact of fast C^{6+} ions and Young-type interference

Saikat Nandi[1], Shubhadeep Biswas[1], Carmen A. Tachino[2], Roberto D. Rivarola[2], and Lokesh C. Tribedi[1,a]

[1] Tata Institute of Fundamental Research, Homi Bhabha Road, Colaba, 400005 Mumbai, India
[2] Laboratorio de Colisiones Atómicas, Facultad de Ciencias Exactas, Ingeniería y Agrimensura, and Instituto de Física Rosario (CONICET-UNR), Avenida Pellegrini 250, 2000 Rosario, Argentina

Received 16 February 2015 / Received in final form 17 February 2015
Published online 4 August 2015 –

Abstract. The absolute Double Differential Cross Sections (DDCS) have been obtained for electron emission from nitrogen molecule under the impact of 72 MeV bare carbon ions. The energy dependence of the electron DDCS was studied for 12 different angles: 20°, 30°, 45°, 60°, 75°, 80°, 90°, 105°, 120°, 135°, 150°, and 160°. At each angle the emitted electrons having energies between 1 and 500 eV were detected. The main interest is to look for the possible existence of interference patterns in the electron spectra due to coherent emission from the two molecular centers. The dynamics of the interaction is described within the continuum distorted wave-eikonal initial state model (CDW-EIS). The DDCS ratios (i.e $N_2/2N$) do not show a clear signature of the oscillatory behavior arising from the interference unlike that observed in the case of H_2. The forward-backward angular asymmetry(α) parameter, as deduced from DDCS values at 30° and 150°, increases monotonically with velocity of the emitted electrons and does show a mild oscillation due to the Young-type electron interference in a molecular double slit. These observations are in qualitative agreement with the prediction of the CDW-EIS model. The apparent absence of the oscillation in the DDCS ratios or a mild oscillation in the α-parameter is qualitatively explained in terms of partial cancellation of contributions arising from different molecular orbitals. The single differential cross sections (SDCS) are well reproduced by the CDW-EIS model as well as the semi-empirical Rudd model. The overall agreement of the DDCS data with the CDW-EIS is extremely good. However, a closer inspection revealed occasional deviations in the angular distribution, particularly in extreme forward and backward angles.

1 Introduction

When a fast, highly charged ion collides with a molecule, a number of inelastic processes can occur. The emission of free electrons from the target, known as the Coulomb ionization process, involves the dominant exchange of energy and is also the most probable process for collision velocities exceeding the orbital velocity of the electron in the target. The main process contributing to the ionization cross-section is known as the soft collision mechanism, in which the electrons are emitted with a large impact parameter. Consequently the cross section reaches a maximum at very low emission energies. For highly charged ions, the electrons ejected from a target molecule, can get influenced by the two Coulombic centers, namely, the receding projectile ion and the residual recoil ion. It is expected that the influence of the two center mechanism would become stronger with increase in the perturbation strength.

In this situation, the ejected electron can undergo a significant amount of successive or simultaneous deflection in the two center fields. Consequently, the cross-sections in the forward angles get enhanced due to the strong attraction of the emitted electrons by the receding projectile ions moving in the same direction. Evidently, extremely low energy electrons are least affected by the Two Center Effect (TCE), because their velocities are very small compared to that of the projectile ions. These basic processes of electron ejection are extensively studied for low-Z (atomic number) targets such as, H_2, H and He [1–8] and multi-electron atoms, such as, Ne and Xe [9–19].

The two-center (i.e., target atom and projectile nucleus) mechanism has been found to influence the angular distribution of the low-energy electron emission. These distributions are in large disagreement with the calculations predicted from the first-order Born approximation, which deals with the problem in terms of one center model. Such studies are relatively scarce for multi-electronic, multi-orbital targets.

Compared to the atoms, in the case of diatomic molecules, the ionization processes carry the signature of the two-center character of the target wave-function. Investigations on molecular ionization have resulted in the observation of Young-type electron interference in

[a] e-mail: lokesh@tifr.res.in

ionization of a homo-nuclear diatomic molecule. The two-nucleon centers in a homo-nuclear diatomic molecule can be considered as two coherent sources of electrons in molecular ionization. Consequently, the electron that has reached the detector cannot be tagged a priori as from which atom it has been emitted. This phenomenon, similar to Young-type double-slit interference, results in an interference pattern for the measured electron DDCS spectra investigated as a function of the energy of emitted electrons. This was first recognized by Cohen and Fano in 1966 while measuring the photo ionization cross sections of O_2 and N_2 [20]. Later on, Jain and Khare [21] and Jain et al. [22] showed independently the existence of such oscillations in cross section spectrum of electron elastic scattering from hydrogen molecule. The existence of a Young-type interference oscillation in the case of electron emission from H_2 molecules has been established unambiguously, both from experimental [23–32] as well as theoretical [33,34] investigation. Even the existence of a double-frequency component in the oscillatory structure has been debated in the case of ionization of H_2 [35–37].

In recent years, there have been investigations to look for such interference effects in the case of multi-electronic targets such as O_2 and N_2. For example, no interference oscillations due to a molecular double slit were observed in the electron emission spectra for O_2, under impact of bare carbon ions [38,39]. This is in contrast with previous experimental works, one involving ionization of N_2 [40], other for O_2 [41], where (at least a certain type of) oscillations were observed. Similarly, a theoretical work based on ab-initio model calculations for proton impact ionization of N_2 does not reveal any interference patterns in the ionization cross sections [42]. In the present work, a study of the interference effect in case N_2, has been carried out by looking into the DDCS ratios between the molecule and its atomic counterpart (obtained from theoretical calculations), as well as the asymmetry parameter obtained entirely from experimental data. The CDW-EIS calculations for N_2 involves certainly less amount of computational difficulties as compared to O_2, where contributions from both the α and β molecular orbital (depending on the spin of the electron) were considered separately. In the case of N_2, the existence of a paired Highest Occupied Molecular Orbital (HOMO) provides with opportunity to calculate the theoretical cross sections with good accuracy. Here we present a detailed data set of e^--DDCS, SDCS, total cross sections (TCS) for 72 MeV bare carbon ions on a N_2 target, which could provide a stringent test for the theoretical results.

We divide the paper into the following sections: experimental technique, double differential cross sections, two center effect, single differential cross sections, interference oscillation, and conclusion.

2 Experimental techniques

The present experiment was performed using the electron spectroscopy technique. In this approach, the spectra are measured as differentials in both the electron emission energy and solid angle, known as the Double Differential Cross Sections (DDCS). The bare carbon ion projectiles were obtained from the 14-MV BARC-TIFR Pelletron accelerator facility at Mumbai, India. The energy and charge state analyzed C^{4+} ion beam was made to pass through a post accelerator carbon foil stripper to obtain ions of higher charge states, including bare ions. The C^{6+} ions were then selected through the switching magnet and directed to the specific beam-line. The beam was then collimated into the desired size using a pair of four-jawed slits (2×2 mm^2), mounted 1 m apart from each other along the beam-line. These are followed by another aperture of 4 mm diameter. It reduced the probability of producing forward-moving electrons due to slit scattering, which could contribute to the background counts at extreme forward angles. Finally, the beam was passed through a differential pumping arrangement followed by the interaction chamber.

In brief, the scattering chamber consists of a high vacuum chamber equipped with a motorized turntable and a hemispherical electrostatic analyzer for the measurement of angular and energy distributions of ejected electrons [43]. The base vacuum in the chamber was maintained at around 2×10^{-7} Torr or better. The scattering chamber was flooded with the target gas (N_2 molecule) at a suitable pressure (0.15 mTorr) to maintain the single collision condition. The flow of the gas inside the chamber was controlled using a solenoid valve. High purity nitrogen gas, available commercially, was used as the target for the experiment. A capacitance manometer (MKS Baratron) was used to measure the absolute pressure of the target gas inside the chamber. The inner side of the scattering chamber was lined with two sets of thin μ-metal sheets (thickness 0.3 mm) in order to reduce earth's magnetic field to about 5–10 mGauss near the interaction region. The data were collected over a wide angular range of 20°–160°. For a fixed emission angle, the number of electrons at different energies that were ejected in that direction was detected for a specified amount of incident projectile charge collected on a Faraday cup. At each angle, electrons having energies as low as 3 eV, up to 500 eV, were detected. The scanning of voltages on the hemispheres, rotation of the spectrometer and overall data acquisition were carried out with the LabVIEW software and a related National Instrument module (BNC-2120) was used.

3 Double differential cross-sections

The measured energy distributions of absolute DDCS for electron emission from N_2 under the impact of 72 MeV C^{6+} ions have been shown in Figure 1, for six different emission angles. The absolute DDCS data are also provided in tabular form for future reference (see Tab. 1). The error due to statistical fluctuation was low (5–10%) throughout the experiment. The uncertainty in the gas pressure was about 6–7%. Overall, the maximum absolute error in the data presented here is about 15–18%. It is evident that the absolute electron DDCS decreases

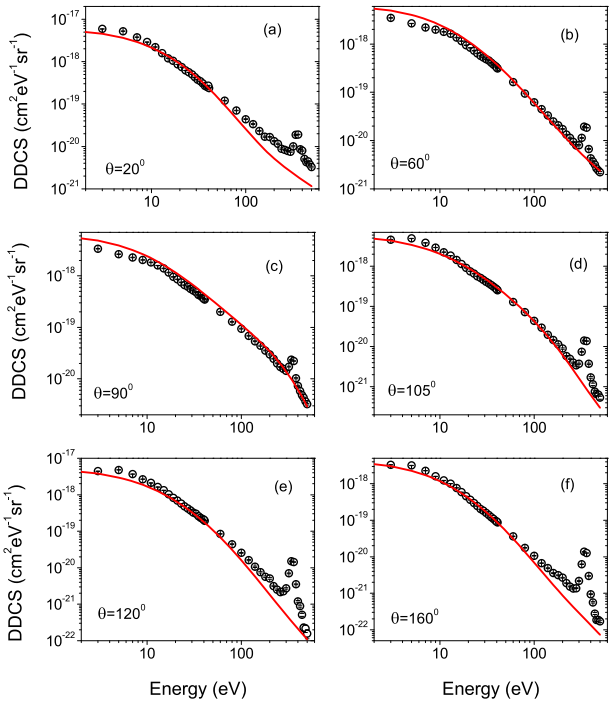

Fig. 1. Absolute electron DDCS for different emission angles for the collision system 72 MeV-C^{6+}+N_2. In each plot, the solid line corresponds to the CDW-EIS calculations.

over three or four orders of magnitude as the energy of the emitted electrons increases between 1 and 500 eV. The emitted electrons in the low energy region are generally produced in soft collisions between the projectiles and the target molecules. These electrons were produced in collisions involving high impact parameter and hence, are emitted with high cross sections. The experimental data were compared with the theoretical calculations using the CDW-EIS model for multi-electronic, di-atomic targets [42].

4 Theoretical methods: comparison with data

Details concerning the theory for single ionization of N_2 molecules by swift ion impact within the two-effective center approximation (TEC) and the CDW-EIS approach, were already given in [42], so only a brief description of the method will be presented here.

It should be noted that, in the case of molecular targets with several molecular orbitals, the active electron can be ionized from any of them. In consequence, the DDCS for the complete molecule, as a function of the energy ε_k and angle θ_k of the emitted electron, should be written as:

$$\sigma^{(2)}(\varepsilon_k,\theta_k) = \sum_{MO} \sigma^{(2)}_{MO}(\varepsilon_k,\theta_k), \qquad (1)$$

with the summation running over all the orbitals of the target. The *partial* DDCS $\sigma^{(2)}_{MO}(\varepsilon_k,\theta_k)$ related to the electron ionization from the Molecular Orbital (MO) can be defined, into the straight line version of the impact parameter approximation and within the CDW-EIS model, as follows:

$$\sigma^{(2)}_{MO}(\varepsilon_k,\theta_k) = \frac{N_{MO}\,k}{4\pi} \times \int d\Omega_{mol} \int d\boldsymbol{\eta}\, |\mathcal{R}^{+\,CDW-EIS}_{if_{MO}}(\boldsymbol{\eta},\Omega_{mol})|^2,$$

where N_{MO} is the corresponding molecular orbital, k is the modulus of the emitted electron momentum $\boldsymbol{k}$, $\boldsymbol{\eta}$ is the transverse component of the momentum transfer $\boldsymbol{q}$, and Ω_{MO} represents the orientation of the target in space. The sign + appearing in the preceding expression refers to the post-form of the scattering matrix element $\mathcal{R}^{+}_{if_{MO}}(\boldsymbol{\eta},\Omega_{mol})$ (see [42] for details about the calculation of this quantity).

In order to describe the active electron bound to a target MO, the corresponding wave function φ_i is expressed as linear combination of Slater-type orbitals ϕ^{STO} centered on each target nucleus:

$$\varphi_i = \sum_{h=1}^{2} \sum_{nlm} \omega_{h,nlm}\, \phi^{STO}_{h,nlm} \qquad (2)$$

where the index h indicates the molecular nuclei where the Slater orbital corresponding to the set of quantum numbers nlm is centered. Then, taken into account equation (2), it can be shown that within the two-effective center (TEC) approach, the scattering matrix element for a given MO can be written as:

$$\mathcal{R}^{+\,CDW-EIS}_{if_{MO}}(\boldsymbol{\eta},\Omega_{mol}) = \sum_{h=1}^{2} \exp[-i\,(\boldsymbol{k}-\boldsymbol{q})\cdot\boldsymbol{b}_h] \times \sum_{nlm} \omega_{h,nlm}\, \mathcal{R}^{+\,eff}_{h,nlm}(\boldsymbol{\eta}) \qquad (3)$$

with $\boldsymbol{b}_h$ the position vector of the h-target center with respect to the origin of a laboratory frame of reference fixed at the center of mass of the molecular nuclei, and $\mathcal{R}^{+\,eff}_{h,nlm}(\boldsymbol{\eta})$ the post version of an *effective* scattering matrix element associated with the Slater function $\phi^{STO}_{h,nlm}$. The DDCS for electron emission in single ionization under the impact of bare carbon ions have been evaluated in the fundamental state $^1\Sigma^+_g$ of N_2 molecule.

The overall shapes of the DDCS spectra, obtained for different emission angles, have been qualitatively well reproduced by the CDW-EIS model, as can be see by the solid curves in Figure 1. As far as the absolute values are concerned, excellent quantitative agreement can be seen between the theory and experimental data from 10 to 300 eV, in the angular range 60°–105°. However, closer inspection reveals that the theoretical values underestimate the data at higher energies (>100 eV), specially at extreme forward and backward angles (see Figs. 1a, 1e, and 1f). The pronounced peak around 340 eV corresponds to the K-LL Auger line for nitrogen. The theoretical model does not take into account the Auger emission process, which is the cause for apparent large quantitative deviations in the higher energy (>300 eV) region.

Table 1. Measured DDCS in units of Mb $eV^{-1}\,sr^{-1}$ for different emission angle. For errors, see the text.

Energy (eV)	20°	30°	45°	60°	75°	80°	90°	105°	120°	135°	150°	160°
3	5.91	4.83	2.16	3.48	3.52	3.26	3.38	4.61	4.42	3.82	3.17	3.30
5	5.20	3.41	1.92	2.66	2.83	2.69	2.63	4.94	4.80	3.85	3.34	3.17
9	2.90	2.00	1.67	1.99	2.19	2.06	2.04	2.92	2.66	1.95	1.66	1.59
11	2.20	1.71	1.51	1.78	1.95	1.82	1.83	2.24	2.11	1.49	1.28	1.23
15	1.20	1.18	1.17	1.36	1.48	1.38	1.40	1.44	1.33	0.98	0.81	0.77
21	0.74	0.66	0.68	0.83	0.88	0.83	0.86	0.75	0.69	0.47	0.38	0.36
25	0.56	0.49	0.53	0.64	0.72	0.66	0.66	0.56	0.48	0.33	0.26	0.24
31	0.38	0.36	0.37	0.49	0.55	0.54	0.52	0.41	0.33	0.22	0.17	0.16
35	0.30	0.30	0.32	0.41	0.48	0.45	0.43	0.34	0.26	0.17	0.13	0.12
40	0.27	0.23	0.25	0.32	0.45	0.37	0.36	0.26	0.21	0.13	0.10	0.092
60	0.12	0.10	0.12	0.16	0.21	0.20	0.20	0.13	0.084	0.051	0.039	0.036
80	0.071	0.057	0.064	0.095	0.14	0.13	0.13	0.072	0.044	0.026	0.019	0.017
100	0.044	0.035	0.040	0.062	0.098	0.097	0.094	0.044	0.026	0.014	0.011	0.011
120	0.034	0.024	0.028	0.045	0.077	0.069	0.069	0.029	0.016	0.0092	0.0072	0.0067
140	0.023	0.017	0.020	0.033	0.058	0.056	0.054	0.020	0.011	0.0063	0.0051	0.0049
160	0.017	0.014	0.014	0.025	0.049	0.046	0.044	0.015	0.0076	0.0046	0.0039	0.0036
180	0.017	0.011	0.012	0.021	0.040	0.042	0.036	0.011	0.0056	0.0037	0.0031	0.0031
200	0.013	0.011	0.011	0.017	0.034	0.034	0.030	0.0090	0.0051	0.0031	0.0026	0.0027
220	0.012	0.0085	0.0079	0.013	0.034	0.031	0.025	0.0058	0.0032	0.0021	0.0016	0.0019
240	0.0089	0.0071	0.0066	0.012	0.025	0.027	0.020	0.0050	0.0025	0.0016	0.0013	0.0015
260	0.0083	0.0067	0.0058	0.0094	0.022	0.024	0.017	0.0040	0.0022	0.0014	0.0012	0.0014
280	0.0079	0.0061	0.0056	0.0080	0.020	0.023	0.016	0.0034	0.0023	0.0016	0.0013	0.0014
300	0.0075	0.0063	0.0048	0.0081	0.019	0.021	0.014	0.0038	0.0027	0.0023	0.0019	0.0022
320	0.010	0.010	0.0093	0.011	0.023	0.024	0.017	0.0074	0.0070	0.0060	0.0053	0.0063
340	0.019	0.019	0.017	0.019	0.029	0.030	0.024	0.014	0.015	0.013	0.012	0.014
360	0.019	0.018	0.016	0.018	0.028	0.030	0.022	0.014	0.014	0.013	0.012	0.013
380	0.0086	0.0063	0.0053	0.0067	0.015	0.017	0.010	0.0037	0.0035	0.0030	0.0028	0.0030
400	0.0080	0.0039	0.0031	0.0043	0.012	0.013	0.0073	0.0017	0.0012	0.00088	0.00085	0.00094
420	0.0051	0.0030	0.0024	0.0037	0.012	0.012	0.0058	0.0012	0.00089	0.00061	0.00052	0.00056
440	0.0043	0.0026	0.0019	0.0032	0.010	0.011	0.0048	0.00075	0.00051	0.00027	0.00023	0.00028
460	0.0045	0.0021	0.0019	0.0027	0.0096	0.010	0.0043	0.00066	0.00023	0.00014	0.00021	0.00019
480	0.0038	0.0020	0.0016	0.0024	0.0088	0.0098	0.0036	0.00064	0.00022	0.00016	0.00015	0.00018
500	0.0033	0.0018	0.0016	0.0022	0.0085	0.0087	0.0032	0.00053	0.00016	0.000093	0.00014	0.00017

5 Angular distribution and angular asymmetry

Figure 2 shows the angular distributions of electron DDCS at different energies of the ejected secondary electrons. In each plot the solid line corresponds to the CDW-EIS calculations. The overall shape of the distributions has been observed to match qualitatively with the CDW-EIS model calculations, considering the complex nature of the target. As it can be seen that at 21 eV, the theory matches with the data only at extreme backward angles (see Fig. 2a). At 60 eV, the theoretical values agree with the data very well over the entire angular range (see Fig. 2b). However, as one increases the emission energy, the discrepancy between theory and experimental data starts to increase. In particular, at very high energy, substantial deviation from the CDW-EIS calculations can be observed, specially at extreme forward and backward angles (see Fig. 2d). It should be noted that in the high energy region the agreement between the theoretical calculations and the experimental data is reasonably good in the intermediate angles,

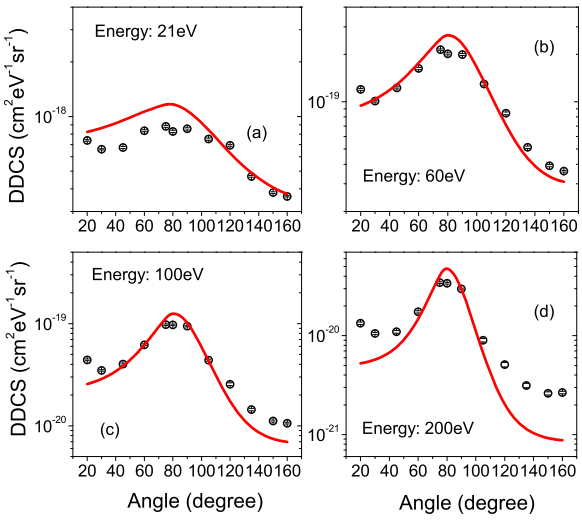

Fig. 2. Absolute electron DDCS for different emission energies. In each plot, the solid corresponds to the CDW-EIS calculations.

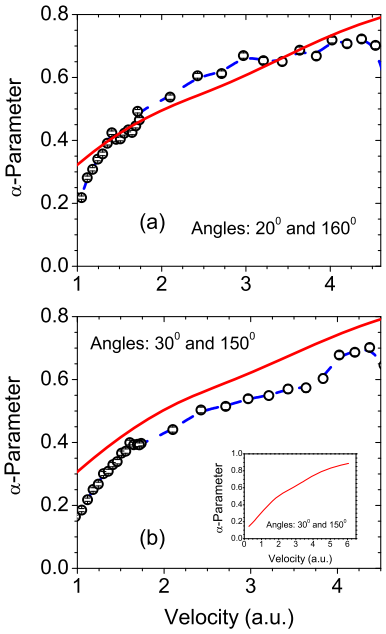

Fig. 3. Variation of α-parameter as a function of electron emission energy. In each plot, the solid red line corresponds to the CDW-EIS calculations. The dashed blue line is only there to guide the eyes.

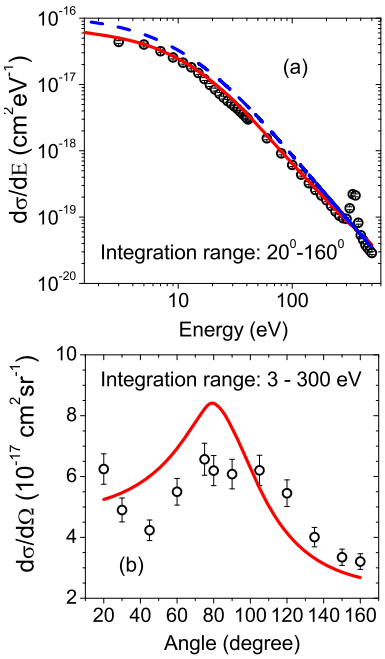

Fig. 4. Absolute electron SDCS as a function of (a) emission energy and (b) emission angle. The solid red line in each plot corresponds to the theoretical calculation using the CDW-EIS model. The dashed blue line in (a) corresponds to the theoretical calculation using the semi-empirical Rudd model [47].

i.e., between 60° to 105° (see Figs. 2c and 2d). The angular distributions at fixed emission energies, as shown in Figure 2, show prominent forward-backward angular asymmetry due to the two-center effect. The enhancement of the cross-section in the forward angles can be attributed to the strong attraction of the emitted electrons by the receding projectiles moving in the same direction. Also, for higher-energy electrons the distributions gradually become more peaked around 75° which is due to the binary nature of collisions [44]. In order to quantify the forward-backward angular asymmetry, arising from the two center effect, one can introduce the parameter $\alpha(k)$ as [45]:

$$\alpha(k,\theta) = \frac{\sigma^{(2)}(k,\theta) - \sigma^{(2)}(k,\pi-\theta)}{\sigma^{(2)}(k,\theta) + \sigma^{(2)}(k,\pi-\theta)}, \qquad (4)$$

where θ is the angle with respect to the direction of the projectile beam in which the electron was emitted with a velocity of k (in a.u.) and $\sigma^{(2)}(k,\theta)$ is the DDCS at that k and θ. Evidently, it represents the importance of the asymmetric contributions. Since the angular distribution varies slowly near 0 and π, we have used the DDCS measured at 20° and 160° and 30° and 150° to obtain the approximate value of the $\alpha(k,\theta)$. Figure 3a shows the velocity dependence of the angular asymmetry parameter at $\theta = 20°$. In this case, the α parameter varies from 0.2 to 0.7 over an energy range of 10 eV to 300 eV for ejected electrons. Similarly Figure 3b shows the velocity dependence of the angular asymmetry parameter at $\theta = 30°$. Once again, the α parameter varies from 0.2 to 0.7 over an energy range of 10 eV to 300 eV for ejected electrons. The theoretical values match quite well in the case of the asymmetry parameter at $\theta = 20°$. However, it should be noted that at $\theta = 30°$ the amount of asymmetry, as predicted by the CDW-EIS model overestimates that obtained from the experiment, throughout the entire range of emission energy. The asymmetry parameter, both from theory as well as from experimental data, is found to increase monotonically with electron velocity. This feature, in general, can be explained in terms of a two-center effect as described earlier [6,7,46]. In addition, the non-Coulombic nature of the target potential can also play a significant role in the forward-backward asymmetry. However a closer look shows an indication of mild oscillation. It is slightly more obvious in Figure 3b i.e. for α-parameter derived from 30° and 150°.

6 Single differential cross sections

The single differential cross-sections, $\frac{d\sigma}{dE}$, obtained by integrating the DDCS (both experimental and theoretical) in an angular range of $20° - 160°$, have been shown in Figure 4a. It can be seen that the CDW-EIS model has qualitatively well reproduced the data. As far as the absolute values are concerned, one can find excellent agreement over the entire energy range, from 3 to 300 eV. In the region containing the Auger emission of N_2 some deviations can be seen between the data and the experimental data. The corresponding SDCS values as a function of emission energies are tabulated in Table 2. Similarly, the single differential cross-sections, $\frac{d\sigma}{d\Omega}$, obtained by integrating the DDCS (both experimental and theoretical) in an energy range of 3–300 eV, has been shown in Figure 4b.

Table 2. Experimental $\frac{d\sigma}{dE}$ values in units of Mb/eV.

Energy (eV)	SDCS	Energy (eV)	SDCS	Energy (eV)	SDCS	Energy (eV)	SDCS	Energy (eV)	SDCS	Energy (eV)	SDCS
3	43.8	5	40.0	9	25.6	11	21.4	15	15.0	21	8.40
25	6.34	31	4.68	35	3.89	40	3.12	60	1.55	80	0.92
120	0.44	140	0.33	160	0.26	180	0.21	200	0.18	220	0.15
100	0.61	240	0.12	260	0.105	280	0.096	300	0.094	320	0.14
340	0.22	360	0.21	380	0.082	400	0.053	420	0.045	440	0.038
460	0.034	480	0.031	500	0.029						

Table 3. Experimental $\frac{d\sigma}{d\Omega}$ values in units of Mb/sr.

20°	30°	45°	60°	75°	80°	90°	105°	120°	135°	150°	160°
62.5	49.0	42.3	55.0	65.7	62.0	60.8	62.0	54.5	40.1	33.5	32.0

Table 4. Parameters for fitting the SDCS values to the Rudd model (taken from [49]).

A_1	1.05	B_1	12.0	C_1	0.74	D_1	−0.39	E_1	0.80
A_2	0.95	B_2	1.20	C_2	1.00	D_2	1.30	γ	0.70

Evidently the CDW-EIS model mostly overestimates the data in the forward angles, whereas, at the backward angles it underestimates the data. As the cross sections in the Auger emission region are much less than that of single ionization cross sections dominated by the soft collision processes in the low energy region, the integration over the DDCS has been performed excluding the emission energies >300 eV. The corresponding SDCS values as a function of emission angles are tabulated in Table 3. In addition to the ab-initio model such as the CDW-EIS model, we have compared the $\frac{d\sigma}{dE}$ as obtained from the data with the semi-empirical Rudd model as well [47]. This model is based on a binary encounter approximation modified to agree with the Bethe theory at high energies and with the molecular promotion model at low energies [48]. It assumes that the cross section for ejection of an electron depends only on the emission energy (E), the binding energy of the electron (I), and the projectile velocity.

The analytical expression for the SDCS (for a particular shell in the target) according to Rudd's model is given by [49]:

$$\frac{d\sigma}{dE} = \frac{(S/I)(F_1 + F_2 w)(1+w)^{-3}}{1 + e^{\gamma(w-w_c)/v}}. \tag{5}$$

Here, w is given by, $w = \frac{E}{I}$. The quantity v is given by, $v = \sqrt{\frac{T}{I}}$, in which T is related to the incident projectile energy (T_0) via the relation, $T = (m_e/M_P)T_0$, where m_e denotes the mass of an electron and M_P denotes the mass of the *bare* projectile. The quantity γ is a dimensionless parameter related to the size of the target and w_c is the energy at the kinematic cut-off, given as, $w_c = 4v^2 - 2v - R/4I$, R being the Rydberg energy (13.6 eV). The first term on the right-hand side represents the free electron limit, the second term represents the correction due to electron binding, and the third term gives the correct dependence for $v \ll 1$. The quantities F_1 and F_2 constitute the adjustable parameters in the model, given by:

$$F_1 = L_1 + H_1 \tag{6}$$

and,

$$F_2 = L_2 H_2/(L_2 + H_2) \tag{7}$$

with

$$H_1 = A_1 ln(1+v^2)/(v^2 + B_1/v^2),$$
$$L_1 = C_1 v^{D_1}/(1 + E_1 v^{D_1+4}),$$
$$H_2 = A_2/v^2 + B_2/v^4,$$

and,

$$L_2 = C_2 v^{D_2}.$$

Finally, S is given by, $S = 4\pi a_0^2 N(R/I)^2$, a_0 being the Bohr radius and N being the total number of electrons in the particular shell of the target. The units of $\frac{d\sigma}{dE}$ in equation (5) are determined solely by the choice of units for S and I, since the remaining terms are dimensionless. The ten parameters with required values for the model are tabulated in Table 4. Also, it should be noted that, as the model was developed primarily for proton impact, in the present experiment, the obtained values from equation (5) have been scaled by multiplying them with a factor of Z_P^2, where Z_P is the atomic number of the incident bare projectile. In addition, equation (5) represents the contribution corresponding to one particular shell of the target. For multi-shell target such as the N_2 molecule, contributions from all the orbitals were added in order to calculate the $\frac{d\sigma}{dE}$. Despite being a semi-empirical relation, the Rudd model provides remarkably close agreement with experimental data (see Fig. 4a). While the model overestimates

the data in the region from 3 to 100 eV, the agreement between data and the model improves above 100 eV.

The experimental (theoretical) SDCS values at angles <20° and >160° were extrapolated from the experimental (theoretical) values in the angular range of 20°–160°. The total cross sections (TCS) for ionization obtained from the experimental data is ∼699 Mb, whereas it is ∼743 Mb as predicted by the CDW-EIS model. Finally, the TCS obtained from the Rudd model by integrating numerically the spectrum over 3–300 eV is found to be ∼912 Mb, which is ∼1.3 times higher than that obtained from the experiment.

7 Interference oscillation

7.1 DDCS ratios

For ionization processes involving di-atomic molecules, a secondary electron reaching the detector cannot be tagged as an electron coming from "this" atom or, "that" atom. Hence, the two atoms can act as two sources of coherent matter waves. This two matter waves can interfere, in the same way as two coherent light waves interfere in the case of the Young-type double slit interference, to produce a noticeable oscillatory pattern in the DDCS spectra as a function of the ejected electron velocity [23,24]. Since the effect of interference can be very small to observe accurately, it becomes necessary to divide the DDCS values obtained from the molecular target with those obtained for the atomic target under identical condition. Accordingly, to look for any such effect we have divided our experimental DDCS values for N_2 by two times that for N (keeping same projectile energy, i.e., 72 MeV-C^{6+} for both cases), to look for any such effect. It was shown in an earlier work [50] that, the interference oscillation for electron emission from a H_2 molecule, is proportional to $(1 + \frac{\sin(kcd)}{kcd})$, where k is the electron velocity, $c = c(\theta)$ is the angle dependent frequency parameter and d is the inter-nuclear separation. A variation of c as a function of the emission angle θ can be found elsewhere [32,40]. Evidently, one complete sinusoidal oscillation corresponds to a variation from 0 to 2π for the argument kcd. For fast projectiles and small momentum transfer to the target, one can assume $c(\theta) = 1$ under the dipole approximation. In the case of N_2, we have $d = 2.1$ a.u. and hence, the full oscillation is expected for k varying from 0 to 3 a.u. (i.e., over 0 to 122 eV). We have plotted in Figure 5 the experimental data over a velocity range of 0 to 4 a.u., i.e., excluding the Auger emission region. However, no such behavior could be observed in any of the emission angles. Though some modulation in the experimental DDCS ratios can be seen in the low energy region, specially at the extreme forward angle (see Fig. 5a), it can not be identified as typical oscillations arising from Young-type interference due to its irregularity and absence in the theoretical counterpart depicted by solid lines in Figure 5.

Baran et al. [40] reported earlier on the existence of a secondary oscillation in the case of N_2 under proton impact. They have compared the experimental DDCSs with

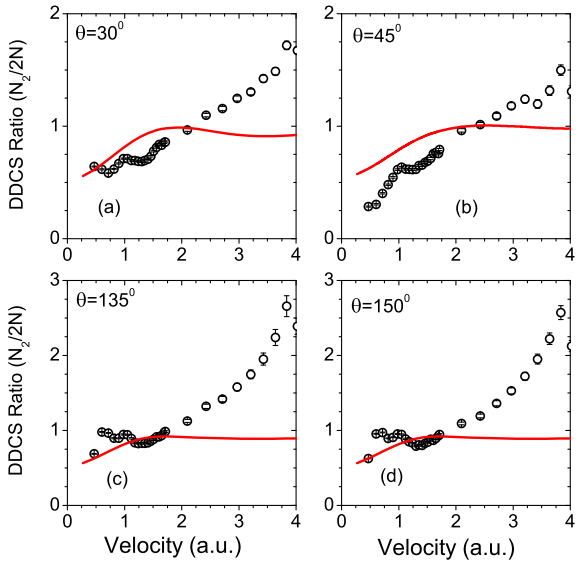

Fig. 5. Ratios of the molecular DDCS for N_2 to 2 times the atomic DDCS for N (obtained from the CDW-EIS model), for four different different angles, 30°, 45°, 135°, 150°. In each plot, the solid line corresponds to the CDW-EIS calculations for the DDCS ratios of $N_2/2N$.

"molecular" calculations using a "monocentric" description of the target orbitals. Thus they obtain the ratio between "normalized" experimental and theoretical results. This ratio was then divided further by a fitted straight line to eliminate the underestimation of the theoretical models compared to the corresponding experimental DDCS at higher electron energies. It should be noted that they did not divide their experimental results by twice the atomic nitrogen DDCS as we have done in the present work.

To understand this behavior, partial DDCS ratios for every orbital of the nitrogen molecule are calculated by dividing the theoretical DDCS for each molecular orbital by twice the DDCS of its atomic counterpart [42]. Figure 6 displays the results of these calculations, as a function of the electron emission energy, at four different emission angles. It can be observed that each MO presents oscillatory structures, which are more pronounced for the higher emission energies. Also, the positions and amplitudes of the corresponding maxima and minima are different. Moreover, these patterns do not present regular oscillations in the considered energy range, and it is evident that the superposition of these spectra gives rise to the apparent absence of interference pattern in the DDCS ratios as shown in Figure 5. A similar conclusion has also been reached from a recent experimental investigation involving photo-ionization of N_2 [51], where oscillations in the $1s\sigma_g$ and $1s\sigma_u$ orbitals are found in opposite phase with respect to each other.

7.2 Angular asymmetry parameter

However, it can be noticed that, this particular way of deriving interference oscillation is heavily dependent on theoretical calculations and normalization procedures.

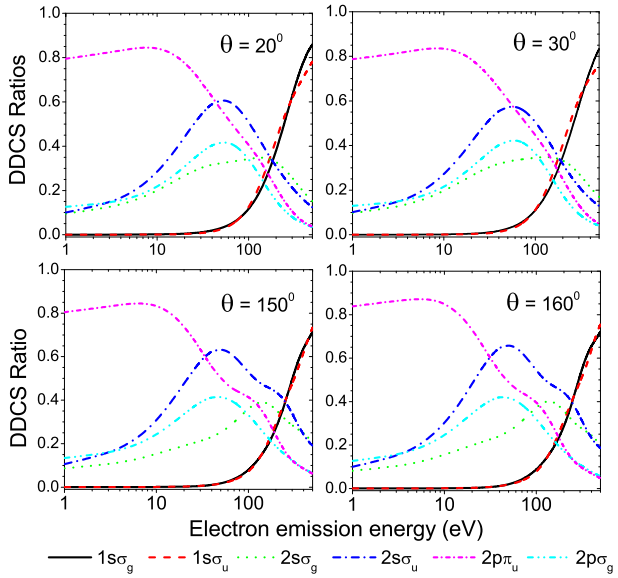

Fig. 6. Theoretical DDCS ratios corresponding to each MO of the target as a function of the electron emission energy for the impact of bare carbon ions at 72 MeV at four different emission angles. The legends describing contributions from each MO are mentioned at the bottom of the figure.

The apparent oscillatory structure present in Figure 5 may be an artifact of the model used to obtain the atomic cross sections. In order to investigate the presence of interference oscillations from the experimental data only, one may use the α-parameter (Fig. 3, discussed earlier). It can be seen that the α-parameter derived from $\theta = 20°$ and 160° does not show a proper oscillation. However, from Figure 3b, one may notice a feeble oscillatory behavior riding on top of the monotonically increasing function. Thus the α-parameter is probably more sensitive to display such interference oscillation present in the spectrum. For the H_2 molecule, a prominent oscillatory behavior was observed earlier, in the the velocity dependence of the asymmetry parameter [32,50,52]. This particular phenomenon in case of H_2 is well understood in terms of the Cohen-Fano model for oscillations in e-DDCS spectrum in the case of diatomic molecules. Although nitrogen is a diatomic molecule, the reason for the absence of an oscillatory behavior or the presence of a mild oscillations in the α-parameter can be attributed to the several molecular orbitals present in N_2. The contribution from each MO are phase shifted so that, when added, all them tend to cancel each other, partially or fully, resulting in no oscillation in some cases or a mild oscillation.

8 Conclusion

We have measured the absolute double differential, single differential and total ionization cross sections for electron emission from a diatomic molecule, N_2, in collisions with 72 MeV bare carbon ions. The forward-backward asymmetry parameter spectrum was also investigated from the measured angular distribution. The CDW-EIS model calculations using a suitable molecular wavefunction compare very well with the details of the energy and angular distributions of the measured electron DDCS. Apart from the different physical processes, such as, soft collision mechanism, two-center effect and binary encounter mechanisms, the possible existence of oscillations in the spectrum due to the Young-type interference effect was also investigated. Although no clear signature has been observed in the DDCS ratios, a low amplitude oscillation can be seen in certain forward-backward angular asymmetry parameter which can be considered as a more sensitive parameter to look for the oscillation. Each independent orbital in nitrogen molecule has been shown to contain oscillatory structures due to Young-type interference, which are phase shifted from each other. A mutual cancellation, partial or full, of the contributions from different orbitals thus give rise to no oscillation in the DDCS ratios or mild oscillation in the forward-backward asymmetry parameter.

We would like to thank the staff at BARC-TIFR Pelletron accelerator facility for smooth operation of the machine. LCT had developed idea and designed the research, SN and SB collected the data, SN analyzed the data, CAT and RDR provided the theoretical calculations, SN and LCT wrote the paper with inputs from CAT and RDR.

References

1. N. Stolterfoht, R.D. DuBois, R.D. Rivarola, *Electron Emission in Heavy Ion-Atom Collisions* (Springer-Verlag, Berlin, 1997)
2. L.H. Toburen, N. Stolterfoht, P. Ziem, D. Schneider, Phys. Rev. A **24**, 1741 (1981)
3. C. Liao, P. Richard, S.R. Grabbe, C.P. Bhalla, T.J.M. Zouros, S. Hagmann, Phys. Rev. A **50**, 1328 (1994)
4. R.D. DuBois, L.H. Toburen, M.E. Middendorf, O. Jagutzki, Phys. Rev. A **49**, 350 (1994)
5. Y.D. Wang, L.C. Tribedi, P. Richard, C.L. Cocke, V.D. Rodriguez, C.D. Lin, J. Phys. B **29**, L203 (1996)
6. L.C. Tribedi, P. Richard, D. Ling, Y.D. Wang, C.D. Lin, R. Moshammer, G.W. Kerby III, M.W. Gealy, M.E. Rudd, Phys. Rev. A **54**, 2154 (1996)
7. L.C. Tribedi, P. Richard, Y.D. Wang, C.D. Lin, R.E. Olson, Phys. Rev. Lett. **77**, 3767 (1996)
8. L.C. Tribedi, P. Richard, W. DeHaven, L. Gulys, M.W. Gealy, M.E. Rudd, J. Phys. B **31**, L369 (1998)
9. R.K. Cacak, T. Jr. Jorgensen, Phys. Rev. A **2**, 1322 (1970)
10. J.B. Crooks, M.E. Rudd, Phys. Rev. A **3**, 1628 (1971)
11. P.H. Woerleet, Yu. S. Gordeev, H. de Waard, F.W. Saris, J. Phys. B **14**, 527 (1981)
12. G. Bernardit, P. Fainstein, C.R. Garibottii, S. Suárez, J. Phys. B **23**, L139 (1990)
13. T.J. Gay, M.W. Gealy, M.E. Rudd, J. Phys. B **23**, L823 (1990)
14. R.D. DuBois, S.T. Manson, Phys. Rev. A **42**, 1222 (1990)
15. S. Suárez, C. Garibotti, W. Meckbach, G. Bernardi, Phys. Rev. Lett. **70**, 418 (1993)
16. S. Suárez, C. Garibotti, G. Bernardi, P. Focke, W. Meckbach, Phys. Rev. A **48**, 4339 (1993)

17. M. Kuzel, R.D. DuBois, R. Maier, O. Heil, D.H. Jakubassa-Amundsen, M.W. Lucas, K.O. Groeneveld, J. Phys. B **27**, 1993 (1994)
18. S. Biswas, D. Misra, J.M. Monti, C.A. Tachino, R.D. Rivarola, L.C. Tribedi, Phys. Rev. A **90**, 052714 (2014)
19. S. Biswas, S. Kasthurirangan, D. Misra, J.M. Monti, R.D. Rivarola, P.D. Fainstein, L.C. Tribedi, Phys. Rev. A **91**, 022711 (2015)
20. H.D. Cohen, U. Fano, Phys. Rev. **150**, 30 (1966)
21. D.K. Jain, S.P. Khare, Phys. Lett. A **63**, 237 (1977)
22. A. Jain, A.N. Tripathi, M.K. Srivastava, Phys. Rev. A **20**, 2352 (1979)
23. N. Stolterfoht, B. Sulik, V. Hoffmann, B. Skogvall, J.Y. Chesnel, J. Rangama, F. Frémont, D. Hennecart, A. Cassimi, X. Husson, A.L. Landers, J.A. Tanis, M.E. Galassi, R.D. Rivarola, Phys. Rev. Lett. **87**, 023201 (2001)
24. D. Misra, U. Kadhane, Y.P. Singh, L.C. Tribedi, P.D. Fainstein, P. Richard, Phys. Rev. Lett. **92**, 153201 (2004)
25. J.A. Tanis, S. Hossain, B. Sulik, N. Stolterfoht, Phys. Rev. Lett. **95**, 079301 (2005)
26. D. Misra, U. Kadhane, Y.P. Singh, L.C. Tribedi, P.D. Fainstein, P. Richard, Phys. Rev. Lett. **95**, 079302 (2005)
27. F. Frémont, A. Hajaji, A. Naja, C. Leclercq, J. Soret, J.A. Tanis, B. Sulik, J.-Y. Chesnel, Phys. Rev. A **72**, 050704(R) (2005)
28. J.A. Tanis, J.Y. Chesnel, B. Sulik, B. Skogvall, P. Sobocinski, A. Cassimi, J.-P. Grandin, L. Adoui, D. Hennecart, N. Stolterfoht, Phys. Rev. A **74**, 022707 (2006)
29. D. Misra, A. Kelkar, U. Kadhane, A. Kumar, Y.P. Singh, Lokesh C. Tribedi, P.D. Fainstein, Phys. Rev. A **75**, 052712 (2007)
30. L. Ph. H. Schmidt, S. Schössler, F. Afaneh, M. Schöffler, K.E. Stiebing, H. Schmidt-Böcking, R. Dörner, Phys. Rev. Lett. **101**, 173202 (2008)
31. D. Misra, A.H. Kelkar, Lokesh C. Tribedi, C.R. Stia, O.A. Fojón, R.D. Rivarola, Phys. Rev. A **78**, 052701 (2008)
32. S. Chatterjee, D. Misra, A.H. Kelkar, P.D. Fainstein, L.C. Tribedi, J. Phys. B **43**, 125201 (2010)
33. M.E. Galassi, R.D. Rivarola, P.D. Fainstein, N. Stolterfoht, Phys. Rev. A **66**, 052705 (2002)
34. L. Nagy, L. Kocbach, K. Póra, J.P. Hansen, J. Phys. B **35**, L453 (2002)
35. N. Stolterfoht, B. Sulik, B. Skogvall, J.Y. Chesnel, F. Frémont, D. Hennecart, A. Cassimi, L. Adoui, S. Hossain, J.A. Tanis, Phys. Rev. A **69**, 012701 (2004)
36. N. Sisourat, J. Caillat, A. Dubois, P.D. Fainstein, Phys. Rev. A **76**, 012718 (2007)
37. D. Misra, A.H. Kelkar, S. Chatterjee, L.C. Tribedi, Phys. Rev. A **80**, 062701 (2009)
38. S. Nandi, A.N. Agnihotri, S. Kasthurirangan, A. Kumar, C.A. Tachino, R.D. Rivarola, F. Martín, L.C. Tribedi, Phys. Rev. A **85**, 062705 (2012)
39. S. Nandi, A.N. Agnihotri, C.A. Tachino, R.D. Rivarola, F. Martín, L.C. Tribedi, J. Phys. B **45**, 215207 (2012)
40. J.L. Baran, S. Das, F. Járái-Szábo, K. Póra, L. Nagy, J.A. Tanis, Phys. Rev. A **78**, 012710 (2008)
41. M. Winkworth, P.D. Fainstein, M.E. Galassi, J.L. Baran, B.S. Dassanayake, S. Das, A. Kayani, J.A. Tanis, Nucl. Ins. Meth. Phys. Res. B **267**, 373 (2009)
42. C.A. Tachino, F. Martín, R.D. Rivarola, J. Phys. B **45**, 025201 (2011)
43. D. Misra, K.V. Thulasiram, W. Fernandes, A.H. Kelkar, U. Kadhane, A. Kumar, Y.P. Singh, L. Gulyas, L.C. Tribedi, Nucl. Ins. Meth. Phys. Res. B **267**, 157 (2009)
44. S.T. Manson, L.H. Toburen, N. Stolterfoht, Phys. Rev. A **12**, 60 (1975)
45. P.D. Fainstein, L. Gulyás, F. Martín, A. Salin, Phys. Rev. A **53**, 3243 (1996)
46. L.C. Tribedi, P. Richard, L. Gulyas, M.E. Rudd, Phys. Rev. A **63**, 062724 (2001)
47. M.E. Rudd, Nucl. Tracks Radiat. Meas. **16**, 213 (1989)
48. M.E. Rudd, Phys. Rev. A **38**, 6129 (1988)
49. M.E. Rudd, Y.-K. Kim, D.H. Madison, T.J. Gay, Rev. Mod. Phys. **64**, 441 (1992)
50. D. Misra, A. Kelkar, U. Kadhane, A. Kumar, L.C. Tribedi, Phys. Rev. A **74**, 060701(R) (2006)
51. M. Ilchen, L. Glaser, F. Scholz, P. Walter, S. Deinert, A. Rothkirch, J. Seltmann, J. Viefhaus, P. Decleva, B. Langer, A. Knie, A. Ehresmann, M. Braune, G. Hartmann, A. Meissner, L. Tribedi, M. Al-Khaldi, O. Al-Dossary, U. Becker, Phys. Rev. Lett. **112** 023001 (2014)
52. S. Chatterjee, D. Misra, A.H. Kelkar, P.D. Fainstein, L.C. Tribedi, J. Phys.: Conf. Ser. **163**, 012074 (2009)